Nucleic Acids Research, 2025, **53**, gkaf229
https://doi.org/10.1093/nar/gkaf229
Gene regulation, Chromatin and Epigenetics

N4-acetylcytidine coordinates with NP1 and CPSF5 to facilitate alternative RNA processing during the replication of minute virus of canines

Xueyan Zhang[1,2], Shuangkang Qin[1,3], Fang Huang[2], Haizhou Liu[1], Jun Wang[1], Zhen Chen[1], Haojie Hao[1,2], Shuang Ding[1], Lishi Liu[2], Baocheng Yu[1,3], Yi Liu[2], Haibin Liu[1,2], Wuxiang Guan[1,2,*]

[1]Center for Emerging Infectious Diseases, Wuhan Institute of Virology, Center for Biosafety Mega-Science, Chinese Academy of Sciences, Wuhan, Hubei 430071, China
[2]Hubei Jiangxia Laboratory, Wuhan, Hubei 430200, China
[3]University of Chinese Academy of Sciences, Beijing 100049, China
[*]To whom correspondence should be addressed. Email: guanwx@wh.iov.cn

Abstract

RNA modifications play crucial roles in RNA metabolism, structure, and functions. N4-acetylcytidine (ac4C) modifications have been shown to enhance stability and translation efficiency of messenger RNAs and viral RNAs. However, the relationship between ac4C and alternative RNA processing remains unexplored. Here, N-acetyltransferase 10 (NAT10) and its catalyzed ac4C modifications on minute virus of canines (MVC) were shown to regulate viral DNA replication and RNA processing, including both the alternative RNA splicing and polyadenylation. Through acRIP-seq and RedaC:T-seq, functional ac4C-modified residue 3311 was identified and characterized, which affected MVC RNA processing rather than altered the viral RNA stability. Ac4C modification at nt 3311 was revealed to participate in NP1-mediated viral RNA processing without influencing RNA affinity of NP1. Meanwhile, CPSF5 was identified to interact with NP1 and mediate viral RNA processing in an ac4C-dependent manner. Further *in vitro* assays showed that NP1 recruited CPSF5 to MVC RNAs, and the ac4C modification promoted specific binding of CPSF5 to the target region, which ensured precise alternative MVC RNA processing. This study not only reveals the functions of NAT10 and ac4C but also elucidates the mechanisms by which RNA modifications orchestrate MVC proteins and host factors for efficient viral replication and alternative RNA processing.

Graphical abstract

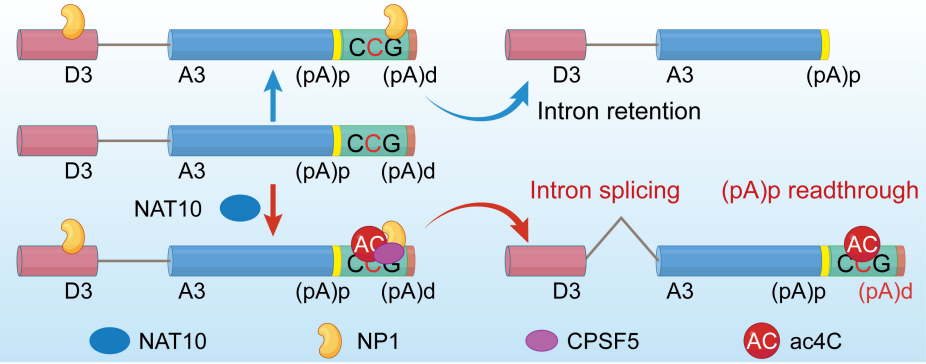

Introduction

Post-transcriptional modifications of messenger RNAs (mRNAs) significantly contribute to RNA metabolism and functional regulation [1, 2]. Several RNA modifications, such as N6-methyladenosine (m6A) and 5-methylcytosine (m5C), along with related host factors, regulate RNA processing [3–6], trafficking [7–9], stability [10, 11], and translation efficiency [12, 13]. N4-acetylcytidine (ac4C) is a specific RNA modification found primarily in transfer RNA (tRNA) [14–17] and, to a lesser extent, in other RNA types, including mRNAs [15, 16], ribosomal RNA (rRNA) [17], and so on. Recently, it has been shown to influence the translation

Received: November 13, 2024. **Revised:** February 7, 2025. **Editorial Decision:** March 6, 2025. **Accepted:** March 12, 2025

efficiency and fidelity of mRNAs, affecting how effectively tRNAs pair with codons during protein synthesis [18]. Dysregulation of ac4C modification has been reported in certain diseases [19, 20], including cancer [21, 22], highlighting its importance in maintaining cellular homeostasis. N-acetyltransferase 10 (NAT10) acts as an acetyltransferase, specifically acetylating the nitrogen at position 4 of cytidine residues, leading to the formation of ac4C [17]. It is the primary enzyme responsible for introducing the ac4C modification in tRNA [23], rRNA [17], and mRNA [15, 18]. However, whether ac4C modifications participate in alternative RNA splicing or polyadenylation remains unclear.

The minute virus of canines (MVC) belongs to the *Bocaparvovirus* genus within the *Parvoviridae* family and is a small, non-enveloped, single-stranded DNA virus containing a 5402 nt linear genome flanked by terminal palindrome sequences [24–26]. MVC generates a single pre-mRNA from a promoter at the left end of the genome (P6) [24, 27]. This is processed via alternative splicing and alternative polyadenylation into multiple nonstructural and capsid-encoding transcripts that are used to produce four viral proteins: two non-structural proteins, NS1 and NP1, and two structural proteins, VP1 and VP2 [24, 26]. NS1 features DNA-binding and endonuclease domains at its N-terminus, ATPase, and helicase domains in the central region, and a transactivation domain at the C-terminus. These domains are crucial for viral replication as they interact with various host factors [28, 29]. NP1 regulates alternative polyadenylation and splicing of MVC pre-mRNAs and controls expression of structural proteins during the viral replication [30, 31]. But the detailed mechanisms how NP1 coordinates with other viral proteins and host factors to maintain such fine-tuned process remain limitedly explored.

MVC RNA processing, including three different splicing manners and two different polyadenylation ways, determines proper mature mRNA levels of non-structural and capsid proteins for efficient infection. Numerous studies indicate that the whole viral RNA processing relies on the coordination between the *trans*-acting splicing factors/complexes, *cis*-acting RNA elements, and other potential machineries. NP1 is essential for efficient read-through of the internal polyadenylation site (pA) and splicing at the adjacent 3D site. The RNA-binding ability of NP1 and the arginine/serine (SR) dipeptide motifs ensure the precise processing of viral RNA [30, 32]. A recent study revealed that NP1 interacts with CPSF6, which facilitates the nuclear import of NP1 and participates in NP1-mediated viral RNA processing [32]. While, the precise mechanisms underlying the NP1-mediated initiation of viral RNA processing remain unexplored. Nevertheless, RNA modifications have been reported to participate in the host/viruses RNA processing [33–35]. These provide a potential regulatory pathway that the undefined RNA modifications in the RNA *cis*-elements nearby the RNA processing sites are involved in the MVC RNA maturation process.

ac4C modifications have been detected in various viruses, including Zika virus, dengue virus, hepatitis C virus, poliovirus, human immunodeficiency virus type 1 (HIV-1), and influenza A virus [36, 37]. This modification boosts HIV-1 RNA translation efficiency and stability [38], enhances enterovirus 71 RNA translation and pathogenicity [39], and stabilizes the long non-coding RNA of Kaposi's sarcoma-associated herpesvirus (KSHV), contributing to virus reactivation [40, 41]. Despite these findings, further investigations are needed to reveal the mechanisms underlying ac4C modifications and their roles in viral and host mRNA. In this study, we characterized the roles of ac4C and NAT10 in MVC replication and elucidated the mechanism by which ac4C coordinates viral proteins and host factors to regulate viral RNA processing.

Materials and methods

MVC virus and cells

The original MVC (GA3) and WRD cells were a kind gift from Dr Jianming Qiu of the University of Kansas Medical Center. HEK293T (ATCC, CRL-11268) and WRD cells were cultured in Dulbecco's modified Eagle's medium (Gibco) containing 10% fetal bovine serum at 37°C with 5% CO_2. Cells were treated with 50 μM remodelin (SML1112, Sigma–Aldrich, St. Louis, MO, USA) for 4 h before MVC infection.

MVC was propagated in WRD cells and harvested as previously described [24, 42]. The viral DNA was extracted using a TIANamp virus DNA/RNA kit (Tiangen) according to the manufacturer's instructions, and the copy number was quantified via real-time qPCR using the SYBR Green Master Mix kit (Yeasen Biotech Co., Shanghai, China) with a forward primer 5′-AGG ACC ATC GCT TGG ATA CAT T-3′ and reverse primer 5′-TAC TGG TCC GAG GGC TTG TT-3′. The WT (pIMVC-WT) plasmid was used to generate the standard curve.

Plasmid construction

Flag-epitope-tagged NP1, CPSF5, and NAT10 and HA-epitope-tagged NP1 plasmids were constructed by inserting the coding sequences of NP1, CPSF5, and NAT10 into pXJ40-Flag, p3XFlag-CMV-14, and pXJ40-HA (Sigma–Aldrich). NAT10-mut was constructed by mutating the amino acids G641 to E641 [43] using the ClonExpress II One Step Cloning Kit (Vazyme, Biotech Co., Ltd.). The mutant infectious clones 564–588m, 1689m, 3978m, and 3311m were constructed by substituting the indicated ac4C sites or negative control site based on the MVC infectious clone WT [24]. SRm and 3311m-SRm were constructed by mutating the triple arginine/serine (SR) dipeptide motifs of the NP1 based on the MVC infectious clones WT and 3311m (Supplementary Table S5).

shRNA knockdown

The indicated gene-specific short hairpin RNA (shRNA) sequences were cloned into the pLKO.1-TRC vector (Plasmid 10878; Addgene, Cambridge, MA, USA) and then co-transfected into HEK293T cells with psPAX2 and pMD2.G for lentivirus production using the Lipofectamine 2000 reagent (Invitrogen, 11668-019). Cells were infected via lentivirus, along with polybrene (0.75 μg/ml), and stable knockdown cell lines were selected using 1 μg/ml puromycin. The shRNAs used in the study were as follows (Supplementary Table S4): NAT10 (shNAT10-1: 5′-GCT TTC GGG TAC TCC AAT ATC-3′, shNAT10-2: 5′-GCT GCT GCA GAT GTA CTT TGA-3′), CPSF5 (shCPSF5-1: 5′-GGG TCA ACC AGT TCG GCA ACA-3′, shCPSF5-2: 5′-GCG CAT GAG GGA ATT TGA-3′).

Southern blot and Northern blot analyses

Low-molecular-weight (Hirt) DNA was isolated to detect replicating forms of MVC, as described previously [44, 45]. WRD cells, infected with MVC virus or transfected with infectious clones, were lysed with Hirt extraction solution (10 mM Tris, 10 mM Ethylene Diamine Tetraacetic Acid (EDTA), pH 7.5, 0.6% Sodium Dodecyl Sulfate (SDS)), followed by proteinase K (0.5 mg/ml) treatment. The Hirt DNA was extracted using the phenol:chloroform method and separated on a 1% agarose gel followed by transferring to a Hybond-N+ membrane and ultraviolet crosslinking. The membranes were hybridized with a MVC genome probe (nucleotides 1–5402), prepared using the DIG High Prime DNA Labeling and Detection Starter Kit II (Roche) according to the manufacturer's instructions. The signals were detected using a Tanon 5200 ChemiDoc MP imaging system (Tanon Science & Technology, Shanghai, China).

For Northern blotting, total RNA from MVC-infected cells was extracted using TRIzol reagent (Invitrogen, Carlsbad, CA, USA) and run on a 1% agarose gel containing 2.2 M formaldehyde for 9 h at 28 V, followed by transferring to a Hybond-N+ membrane and UV cross-linking. Signals were detected using the same probe used for Southern blotting.

Western blotting and co-immunoprecipitation

WRD cells were lysed using SDS protein sample buffer at 48 h post-transfection or infection, and then, the cell lysates were subjected to 12% SDS–PAGE for electrophoresis and transferred to a nitrocellulose membrane. Indicated proteins were detected using primary mouse monoclonal antibodies against beta-actin (sc47778, Santa Cruz Biotechnology, Dallas, TX, USA) and GAPDH (Cat. No. 60004-1-lg; Proteintech); rabbit polyclonal antibodies against CPSF5 (A4482, ABclonal), NAT10 (13365-1-AP, Proteintech), and Flag (F1804-1 MG, Sigma–Aldrich); anti-HA (66006-1-Ig, Proteintech) and anti-Histone H3 antibodies (Cat. No. GTX122148; GeneTex); and three rabbit polyclonal antibodies against MVC NP1, NS1, and VP2 that were previously generated [24]. Secondary goat anti-mouse IgG and goat anti-rabbit IgG antibodies (AntiGene Biotech GmbH, Stuttgart, Germany) were used with a manufacturer's protocol. Luminescent signals were detected using the ChemiDoc MP imaging system (Tanon Science & Technology, Shanghai, China).

For immunoprecipitation (IP), primary antibodies including IgG, anti-HA, or an anti-Flag antibodies were mixed with cell lysates in IP lysis buffer [50 mM Tris–HCl, pH 7.5, 1 mM Ethylene Glycol Tetraacetic Acid (EGTA), 1 mM EDTA, 1% Triton X-100, 150 mM NaCl, 2 mM dithiothreitol (DTT), protease inhibitors (DI101-02, TransGen)] for overnight at 4°C and then incubated with protein G or protein A agarose for 2 h at 4°C. After six washes using IP wash buffer (50 mM Tris–HCl, pH 7.5, 1 mM EGTA, 1 mM EDTA, 1% Triton X-100, 300 mM NaCl, 2 mM DTT), agarose-coupled proteins were denatured at 95°C for 10 min and subjected to a western blotting assay.

RNase protection assay

RNase protection assay (RPA) was performed as previously described [46]. The detailed sequence of MVC RPA probes were indicated in the Fig. 1F [42]. Briefly, 20 μg of total RNAs isolated from infected or transfected cells were incubated with MVC probes using RPA buffer (80% formamide, 40 mM pipes, pH 6.4, 400 mM NaCl, 1 mM EDTA) at 51°C overnight after denatured at 95°C for 5 min. Then, the mixtures were treated with RNase A and RNase T1 for 1 h at 30°C and digested with proteinase K for 30 min at 37°C. The RPA samples were separated on a 8% urea-PAGE gel, and the signals were detected using a Cyclone Plus (PerkinElmer) and analyzed with OptiQuant™ software.

Formaldehyde-cross-linked RIP and acRIP-seq

RIP was performed as previously described [47]. Briefly, infected or transfected WRD cells were cross-linked with 1% formaldehyde and lysed with RIP buffer (150 mM KCl, 25 mM Tris–HCl pH 7.4, 5 mM EDTA, 0.5 mM DTT, 0.5% NP-40, 100 U/ml RNase inhibitor, 100 μM phenylmethylsulfonyl fluoride, and 1 μg/ml proteinase inhibitors) on ice. After centrifugation, the cell lysates were subjected to IP using IgG, anti-Flag, or indicated antibodies. Isolated RNA was performed for qRT-PCR with gene-specific primers (Supplementary Table S3) using Hieff® qPCR SYBR® Green Master Mix.

The acRIP-seq was performed according to a previously published protocol [15]. Total RNA was extracted from MVC-infected WRD cells and purified using an Oligo (dT) kit (Thermo Scientific, Wilmington, DE, USA). The acRIP was performed by IP using anti-ac4C antibodies and next-generation sequencing. Details are described as GenSeq ac4C RIP Kit according to the manufacturer's instructions. Both the acRIP and input samples were used for library generation using the NEBNext Ultra II Directional RNA Library Prep Kit (New England Biolabs). The library was validated using an Agilent 2100 Bioanalyzer and sequenced on a DNBSEQ-T7. The data of acRIP-seq was analyzed as described previously [42].

RedaC:T-seq and data analysis

RedaC:T-seq was performed by SeqHealth Technology Co., Ltd (Hanwu, China) according to a previously published protocol [48]. Briefly, Total RNA was purified from MVC-infected WRD cells, followed by treatment with DNase I and Poly(A)+ RNA capture using the KAPA mRNA Capture Kit (KK8441) according to the manufacturer's instructions. A small amount of captured RNA was taken as the "Con" sample, and the remaining RNA was treated with 100 mM NaBH4 at 55°C in the dark for 30 min. NaBH4-treated RNA was precipitated using 0.3 M sodium acetate (pH 5.5), 15 mg/ml linear acrylamide (carrier), and 2.5 × ethanol. The KC Digital Stranded mRNA Library Prep Kit from Illumina (DR085-02) was used to construct the library. The kit eliminates duplication bias in the PCR and sequencing steps using a unique molecular identifier (UMI) of eight random bases to label pre-amplified complementary DNA molecules. Library products corresponding to 200–500 bp were enriched, quantified, and sequenced on an MGISEQ-T7 (MGI) with the PE150 model.

Raw sequencing data were filtered using fastp (version 0.23.1), low-quality reads were discarded, reads contaminated with adaptor sequences were trimmed. UMI (version 1.0), self-developed software from Seqhealth Co., Ltd., was used to eliminate duplicates. After duplication removal, the reads were mapped to the reference genome of MVCs from NCBI (FJ214110) using STAR (version 2.7.6a) with default parameters. Sambamba (version 0.7.1) was used for Sam/Bam format conversion and index building. Feature counts (version 1.5.1)

were used for the read distribution statistics. JACUSA software (version 2.0.1) was used to detect SNV sites and obtain the corresponding pile-up. The self-developed software Rigel (version 1.0.0) was used to perform statistical tests on the detected SNV sites and identify differential ac4C sites.

Liquid chromatography tandem MS

The liquid chromatography tandem MS (LC-MS/MS) assays were performed following the standard procedures [49]. Briefly, total RNA was extracted from MVC-infected WRD cells, with following purification of the MVC RNAs by using viral probes [37]. Then, S1 nuclease, alkaline phosphatase, and phosphordiesterase I were introduced into 1 μg viral RNAs, followed with incubation at 37°C for 3 h. Then RNAs were fully digested into nucleosides followed with extraction with chloroform. The resulting aqueous layer was collected for further analysis via LC-MS. RNA modifications contents were detected based on the AB Sciex QTRAP 6500 LC-MS/MS platform (Wuhan Metware Biotechnology Co., Ltd). The MVC probes used in the study were as follows:

MVC-probe	Sequence
MVC-probe1	CCACATATGGAAATTTCAGGATATAAGT ATAAGCAGGAGTAGAAAATT GAGTAAGGTCGTCTAAAGACGCGATTGG AAGCGTCGACATCA
MVC-probe2	TATCTGTTCTATAAGTTTGTTTCCGCCC GATTGACATTCTAACATAACA ACGAGATCGGCGCACCCATTTACAAGGT CTTCATATGTTAA
MVC-probe3	ATGGTTTCGTCCGAACTTGTTCGTTTTC TTGATGGAGTGGTAGCGTTT GGTGTTTCTGGAGAGTCTAAGAGCGAAA AATCGAAGTTAGTG
MVC-probe4	CTCTTTTGCGCCCTATCTTGTCTACTGT TTCCGGCCACTCTTTTAGCA GGAGGAGTGTTTTCTTTTAGATGTGGAG CCAAAATACGTTTA
MVC-probe5	TTTGTGTGTTTCCAATGTATCCAAGCGA TGGTCCTGGCATCCACTG TGATGGCTTGTTATACGGACTGTATCGC GTGTACACGAATTTTC

RNA–protein pulldown assay

WRD cells were transfected with the indicated Flag-CPSF5 and HA-NP1 plasmids and lysed using lysis buffer (20 mM Tris–HCl, pH 7.5, 100 mM NaCl, 1 mM MgCl2, 0.5 mM EDTA, 0.5 mM DTT) at 48 h post-transfection. After brief sonication (10% amplitude pulse-on: 10 s, pulse-off: 20 s), cell lysates were mixed with 5′ biotin-conjugated RNA oligonucleotides and incubated for 2 h at 4°C, followed by the addition of neutravidin beads and rotation overnight at 4°C. The beads were washed with lysis buffer at least three times to remove non-specifically bound proteins, and agarose-coupled proteins were denatured at 95°C for 10 min and subjected to western blotting.

CPSF5 and NP1 proteins were expressed in a prokaryotic expression system and purified using Ni-NTA column. Equal or increasing amounts of purified proteins were incubated with neutravidin beads for 3 h at 4°C. The beads were then washed three times with lysis buffer and boiled in 2 × SDS loading buffer. The pull-down samples were subjected to western blotting.

Immunofluorescence analysis

WRD cells were infected with MVC or transfected with Flag-NAT10 for 24 h. The cells were then fixed in 4% paraformaldehyde for 1 h, permeabilized in 0.2% Triton X-100 for 10 min, and blocked in 3% bovine serum albumin for 1 h at room temperature. After incubation with NAT10 or Flag antibodies overnight at 4°C, the samples were stained with secondary antibodies (Alexa Fluor 488) for 1 h and Hoechst 33258 for 10 min. The images were captured under a PerkinElmer VoX confocal microscope.

In vitro transcription of ac4C-modified RNA

Two complementary single-strand DNA fragments (Supplementary Table S2), based on the motif containing the modified DSE bearing the indicated ac4C modifications (ac4C at residue 3311), were synthesized. The double-stranded oligomer was generated by annealing above two fragments. Then, according to the manufacturer's instructions, the oligomer was set as the template for the following *in vitro* transcription using a MEGAscript T7 Kit (Ambion, Austin, TX, USA), with CTP (ThermoFisher, R0451) or ac4CTP (MedChemExpress, HY-111815) as substrates. Thus, the indicated RNAs with or without ac4C modifications were obtained and proceeded to the following assays.

Dot blotting

Five microgram *in vitro* transcribed RNA with or without ac4C was denatured for 5 min at 75°C and loaded onto Hybond-N+ membranes. The membrane was crosslinked with ultraviolet light and then blocked in 5% milk. ac4C detection was performed using anti-ac4C antibodies (Abcam, Cambridge, UK) according to the manufacturer's protocol. Immunoblot signals were detected using the Tanon-5200 Chemi-Doc MP imaging system.

Quantification and statistical analysis

All data were analyzed using GraphPad Prism software (version 8). Details of the statistical tests used in this study are provided in the corresponding figure legends. Data are presented as the means ± standard errors of the means or means ± standard deviations. Comparisons between two groups were performed using students' unpaired *t*-tests, while comparisons of the decay curves were performed using two-way ANOVA. $P \leq 0.05$ is considered statistically significant.

Results

The MVC RNA contains ac4C modifications and the acetyltransferase NAT10 promotes virus replication and RNA processing

Multiple viruses were found to be regulated by different RNA modifications during the viral replication [47, 50]. To determine whether MVC RNA contains ac4C modifications or the viral replication is regulated by the ac4C and its related machinery, we firstly measured the level of ac4C modification on MVC RNA via ac4C-acetylated RNA immunoprecipitation (acRIP) followed by qRT-PCR or Northern blot assays. Our data found that ac4C modifications were detected in MVC

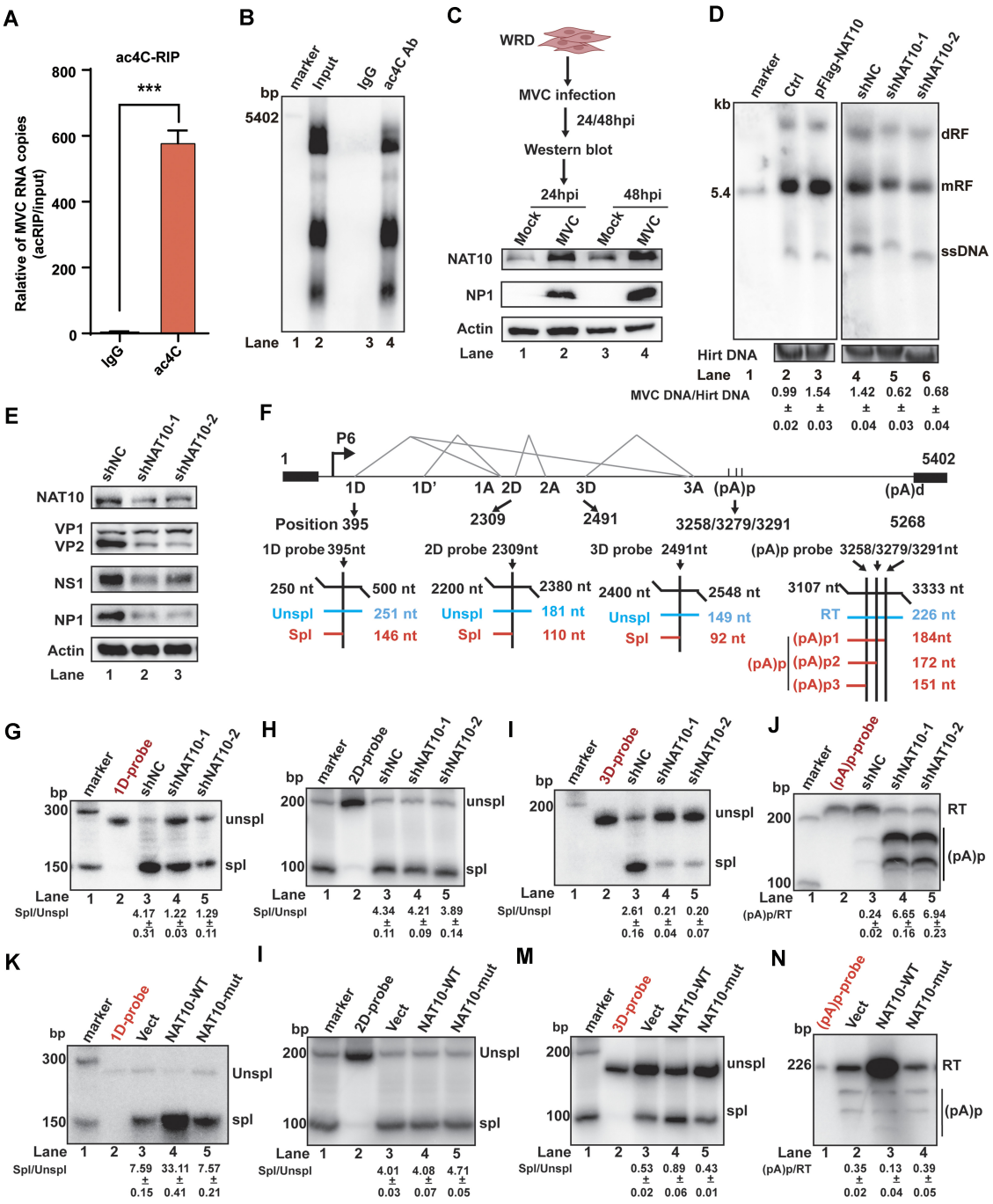

Figure 1. NAT10 promotes MVC replication and affects the alternative viral RNA processing. (**A**) Identification of ac4C on MVC RNA via acRIP (RNA-immunoprecipitation)-qRT-PCR. RNAs from MVC-infected cells were incubated with IgG or anti-ac4C antibodies, followed by IP and qRT-PCR. Data are the means ± SEMs ($n = 3$). $^{***}P \leq 0.001$, unpaired student's *t*-tests. (**B**) The acRIP and Northern blotting. RNAs from MVC-infected WRD cells were incubated with IgG or anti-ac4C specific antibodies as indicated. Immunoprecipitated RNAs were resolved on 1% agarose gels containing 2.2 M formaldehyde and transferred to Hybond-N+ membranes, followed by RNA signal detection with MVC-specific probes spanning from nt 1 to nt 5402. (**C**) Western blot analysis of NAT10 protein expression in MVC-infected cells at 24 h and 48 h post-infection. Actin served as an internal control. (**D**) Southern blot analysis of MVC DNA replication. Hirt DNA was extracted from infected cells with NAT10 overexpression or knockdown and subjected to Southern blot analysis at 48 h post-infection. The MVC full-length probe targeting the 1–5402 region was used for hybridization. EB staining of Hirt DNA served as an internal control. dRF, double replicative form; mRF, monomer replicative form; and ssDNA, single-stranded DNA. (**E**) Western blot analysis of MVC protein expression with NAT10 knockdown from MVC-infected cells at 48 h post-infection. (**F**) The top panel is a diagram of MVC genomic structure, including P6 promoter, four splicing donor sites (1D, 1D′, 2D, and 3D), three accept sites (1A, 2A, and 3A), the proximal polyadenylation cleavage site [(pA)p], and distal polyadenylation cleavage site [(pA)d]. The bottom panel shows the positions and sizes of probes used in RPA. The size of expected RPA products from unspliced RNA (unspl), spliced RNA (spl), RNA utilizing (pA)p site, or (pA)d site is below each probe. (**G**–**J**) Analysis of the alternative splicing of MVC RNA via RPA. Total RNA was extracted from MVC-infected cells in which NAT10 was knocked down at 48 h post-infection using a 1D-probe (**G**), 2D-probe (**H**), 3D-probe (**I**), and (pA)p-probe (**J**) targeting the respective indicated donor sites and (pA)p. Radioactive probes were loaded in each experiment and served as size controls. (**K**–**N**) MVC RNA alternative splicing was measured by mutating the acetylase activity site of NAT10. RPA analysis of MVC RNA processing with NAT10 wild type (NAT10-WT) or G641E (NAT10-mut) mutant overexpression from MVC-infected cells at 48 h post-infection using a 1D-probe (**K**), 2D-probe (**L**), 3D-probe (**M**), and (pA)p-probe (**N**) targeting the respective indicated donor sites and (pA)p.

RNA obtained from the MVC-infected Walter Reed Canine cell/3873D (WRD) cells (Fig. 1A and B). Since MVC did not encode any acetyltransferase or other enzymes with similar functions, the ac4C writer NAT10 was speculated to be responsible for such modification in viral RNA. To confirm this hypothesis, we firstly measured the expression of NAT10 after MVC infection via WB assay. The NAT10 expression was largely increased by the viral infection (Fig. 1C) without affecting its cellular localization (Supplementary Fig. S1A and B), which implied that NAT10 participated in the viral replication. In addition, the MVC RNAs were abundantly enriched by the anti-Flag antibodies in MVC-infected cells with exogenous Flag-NAT10 via the RIP-qPCR assay, compared to the empty vector control. These suggested that NAT10 targeted MVC RNAs for binding (Supplementary Fig. S1C and E). Correspondingly, the following acRIP assays showed that overexpressed NAT10 significantly increased ac4C levels of MVC RNAs pulled down by the anti-ac4C antibodies (Supplementary Fig. S1F). Whereas both inhibition of NAT10 by its specific inhibitor, remodelin, and knocked down by the shRNAs targeting NAT10, greatly decreased the levels of ac4C modified MVC RNAs (Supplementary Fig. S1G and H). Thus, NAT10 potentially acted as the enzyme for the ac4C modifications on MVC RNAs. Moreover, the transfection of a dominant-negative mutant of NAT10, losing its acetyltransferase activities but remaining the RNA binding capabilities, only led to decrease of ac4C levels on viral RNAs (Supplementary Fig. S1I), compared to the empty vector control [51]. Above all, NAT10 was the acetyltransferase responsible for catalyzing ac4C modifications on MVC RNAs.

Subsequently, whether NAT10 could in turn to regulate the MVC replication was investigated. The overexpressed NAT10 was capable to enhance MVC genomic replication measured by the Southern blot assay (Fig. 1D and lanes 1–3). On the contrary, inhibition or depletion of NAT10 as above resulted in much decrease of the viral replication (Fig. 1D, lanes 4–6, and Supplementary Fig. S2A). Recent study revealed that NAT10 facilitates EV71 replication by promoting the translation efficiency and stability of viral RNAs [39]. Here, NAT10 affected RNA transcription and protein expression of MVC (Fig. 1E and Supplementary Fig. S2B–E), but not MVC RNA stability (Supplementary Fig. S3). Thus, NAT10 affects MVC replication.

MVC RNA processing, including the three different alternative RNA splicing manners along with two different RNA polyadenylation ways (Fig. 1F), is essential and sequentially restrained for the effective viral replication [24, 27]. To further characterize the role of NAT10 during the MVC RNA processing, the RPA was performed to analyze the profile of viral RNA processing using indicated probes (Fig. 1F). The depletion (Fig. 1G–J) or inhibition of NAT10 (Supplementary Fig. S4) led to decreased splicing of 1D/1A intron (∼3-fold) (Fig. 1G and Supplementary Fig. S4B) and 3D/3A intron (∼10-fold) (Fig. 1I and Supplementary Fig. S4D) but increased polyadenylation at (pA)p (∼20-fold) (Fig. 1J and Supplementary Fig. S4E) after viral infection, whereas splicing of 2D/2A intron was not affected (Fig. 1H and Supplementary Fig. S4C). The exogenous NAT10 expression exerted opposite effects on the alternative splicing of these different introns (Fig. 1K and M) and polyadenylation at (pA)p of MVC RNAs (Fig. 1N), whereas splicing of 2D/2A intron was not affected (Fig. 1L). In addition, transfection with a mutant NAT10 lacking enzymatic activity [52] did not affect viral RNA processing (Fig. 1K–N). Taken together, NAT10 promoted MVC replication and affected the alternative processing of viral RNAs, which were dependent on its intact enzyme activities.

ac4C facilitates MVC replication, RNA splicing, and polyadenylation

Since the NAT10 catalyzed ac4C modifications on MVC RNAs were involved in the viral replication, the exact and functional ac4C modified residues were further characterized. First, we performed LC-MS/MS assays using the purified MVC RNAs, and ∼0.7% ac4C modified residues among the MVC RNAs were detected (Supplementary Fig. S5A and B) [49]. In addition, through the acRIP-seq assay, ac4C peaks were identified on the region of the MVC genome spanning from nucleotides (nt) 553–600, 2743–3370, 3713–4232 and 4763–4967 (Fig. 2A). To further achieve base-resolution mapping, we conducted sodium borohydride (NaBH4) reduction and the induction of C:T mismatches in sequencing (RedaC:T-seq) [18], and seven potential sites were detected (Fig. 2B). Considering the conserved "C-C-G" motif [53], nucleotides 3311 and 3978 were identified in both sequencing datasets (Fig. 2A and B). Other nucleotides, such as residues 564 and 588, were only detected via RIP-seq. Nucleotide 1689 with CCG motif was not detected and served as a negative control. To characterize the exact ac4C modified residues, the different mutants (3311m, 3978m, 564–588m, 1689m) (Fig. 2C) were constructed to detect the levels of ac4C modifications of MVC RNA by acRIP assay. Only the nucleotide 3311 mutation reduced the ac4C modification level of MVC RNA, which suggested residue 3311 was acetylated (Fig. 2D). To explore whether ac4C modification at residue 3311 affect viral genome replication, Southern blot was performed and revealed that the mutation of nucleotide 3311 reduced MVC replication levels (∼2-fold), whereas no effects were detected in other mutants (Fig. 2E). In addition, the viral VP2 protein expression was inhibited by mutating residue 3311. However, no differences in viral VP2 protein expression were observed among WT and mutant in cells with NAT10 knockdown (Fig. 2F) or treatment with remodelin (Fig. 2H). The NP1 expression was increased (Fig. 2F–H). These results suggested that residues 3311 could be the functional ac4C site to regulate MVC replication.

Along with the viral protein expression affected by mutating residues 3311, the transcription levels of VP2 were also decreased by substituting the nucleotide 3311, compared to WT (Fig. 3A and B). MVC RNA maturation is highly dependent on the alternative viral RNA processing [30]. To confirm whether ac4C site influenced viral RNA processing, WT and other mutants were transfected into cells for RPA analysis. Alternative splicing of the 3D/3A intron was decreased ∼5-fold in cells transfected with 3311m than WT (Fig. 3C, compare lane 6 to lane 3; Fig. 3D, compare lane 4 to lane 3). The enhanced alternative polyadenylation at (pA)p (∼20-fold) was only detected when mutating residue 3311 (Fig. 3E, compare lane 5 to lane 2; Fig. 3F, compare lane 3 to lane 2). Furthermore, no differences in 3D/3A intron RNA splicing (Fig. 3G, compare lanes 7 and 8 to lane 6) and alternative polyadenylation at (pA)p (Fig. 3H, compare lanes 7 and 8 to lane 6) were observed among shNC and NAT10 knockdown in cells with transfection of the mutant 3311m. Above data showed that NAT10-mediated regulation of alternative MVC RNA

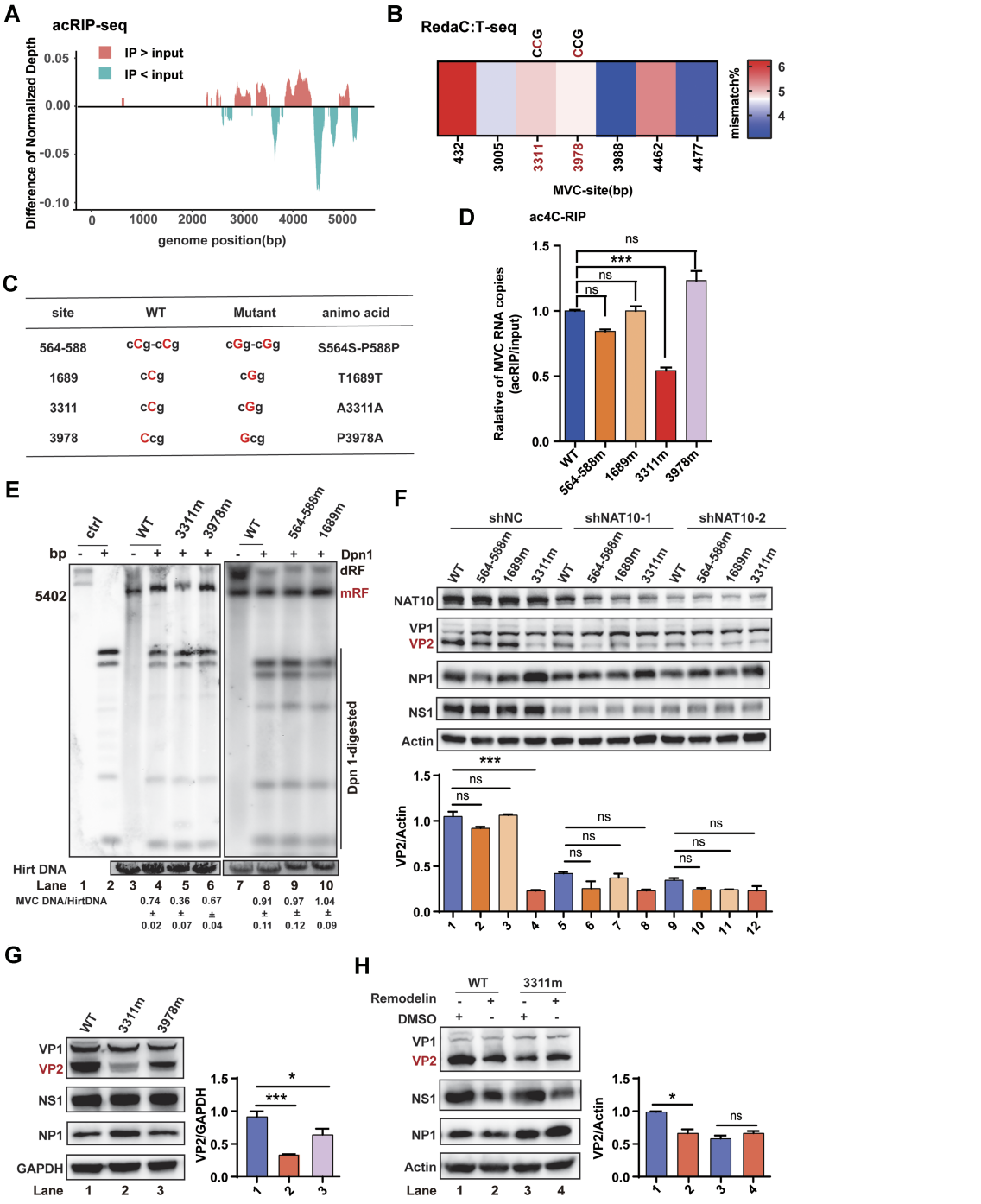

Figure 2. Residues 3311 could be the functional ac4C site to regulate MVC replication. (**A**) Mapping of ac4C sites on MVC RNA via acRIP (RNA-immunoprecipitation)-seq. Poly(A)$^+$ RNA, purified from total RNA extracted from MVC-infected WRD cells, was fragmented, and IP was performed using anti-ac4C antibodies for acRIP-seq, followed by next-generation sequencing. Difference of normalized depth was generated on the coverage of acRIP-seq and input MVC RNA, respectively. (**B**) ac4C sites were detected on MVC RNA via RedaC:T-seq. Poly(A)+ RNA, purified from total RNA extracted from MVC-infected WRD cells, was treated with NaBH4, followed by next-generation sequencing. Both 3311 and 3978 sites were detected in acRIP-seq and RedaC:T-seq with CCG motifs, and only site 3311 was located at the wobble site of the codon. (**C**) The diagram shows the location of ac4C sites and negative control with CCG motif detected in acRIP-seq or RedaC:T-seq. Nucleotides 564–588, 3311, and 3978 were detected as ac4C sites, but 1689 site with CCG motif was not detected and served as a negative control. All mutants are synonymous codon, except 3978 site. (**D**) Identification of ac4C modified MVC RNA by acRIP-qRT-PCR. RNAs from WRD cells transfected with WT and mutant infectious clones were incubated with anti-ac4C antibodies, followed by IP and qRT-PCR. Data are the means ± SEMs ($n = 3$). $^{***}P \leq 0.001$, ns: not significant, unpaired student's *t*-tests. (**E**) MVC DNA replication analysis of cells transfected with WT and mutant infectious clones at 48 h via Southern blotting. EB staining of Hirt DNA served as an internal control. The probe was used as described in Fig. 1**D**. (**F**, **H**) Western blot analysis of MVC protein expression with NAT10 knockdown (**F**) or remodelin treatment (**H**) from WRD cells transfected with WT or the other mutants at 48 h. Actin served as internal control. Relative intensity of VP2 versus actin was quantified using the ImageJ program. Data are means ± SDs ($n = 3$). $^{***}P \leq 0.001$, ns: not significant, unpaired Student's *t*-test. (**G**) Viral proteins expression was detected by western blotting. MVC infectious clones of WT and mutants were transfected into WRD cells and levels of protein were blotted after 48 h post-transfection. GAPDH served as internal control. Relative intensity of VP2 versus GAPDH was quantified using the ImageJ program. Data are means ± SDs ($n = 3$). $^{***}P \leq 0.001$, $^{*}P \leq 0.05$, unpaired Student's *t*-test.

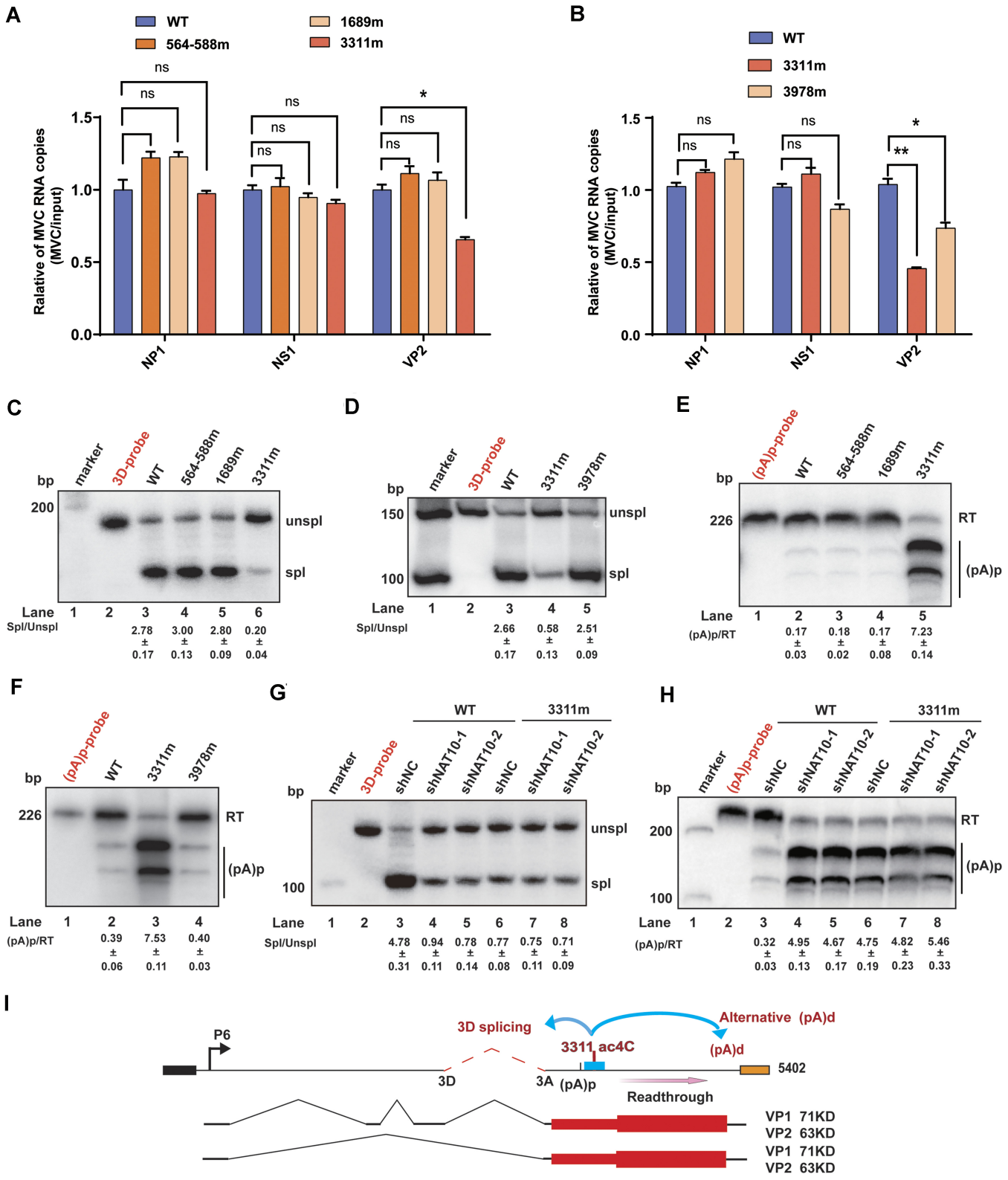

Figure 3. Functional ac4C-modified residue determines the alternative splicing and polyadenylation of MVC pre-mRNAs. (**A**, **B**) qRT-PCR was performed to determine the RNA levels of MVC WT or mutants by NP1, NS1, and VP2 ORF primers in WRD cells at 48 h transfection of infectious clones, and GAPDH was used as a control. Data are means ± SEMs ($n = 3$). $^{*}P \leq 0.05$, $^{**}P \leq 0.01$, ns: not significant, unpaired Student's *t*-tests. (**C**–**F**) Regulation of MVC RNA alternative splicing via the functional ac4C-modified residue. RPA of total RNA extracted from cells transfected with MVC-WT and mutant infectious clones at 48 h was performed using 3D-probe (**C**, **D**) and (pA)p-probe (**E**, **F**). (**G**, **H**) The correlation between acetyltransferase NAT10 and ac4C-modified residues regulated MVC RNA alternative splicing. RPA of total RNA extracted from cells transfected with WT and mutant infectious clones in which NAT10 was knocked down at 48 h was performed using a 3D-probe and (pA)p-probe. (**I**) The model of acetylation at site 3311 regulates alternative 3D/3A RNA splicing and readthrough of (pA)p.

processing relies on ac4C at residue 3311. Collectively, the ac4C-modified residue 3311 participated in MVC replication and in the alternative splicing and polyadenylation of viral RNAs (Fig. 3I).

NP1-mediated 3D/3A splicing and (pA)p polyadenylation rely on ac4C at residue 3311

The viral protein NP1 [30] has been characterized as the regulatory protein to influence the alternative MVC RNA splicing of the 3D/3A intron and the RNA polyadenylation at (pA)p. Above data showed that ac4C at residue 3311 presented similar pattern to the viral RNA processing as NP1. The RNA-binding ability of NP1 maintains the subsequent NP1-mediated viral RNA processing [30, 32], which implied that ac4C at residue 3311 might be involved in NP1 binding to viral RNAs. Thus, we investigate the affinity of NP1 to MVC RNA with or without ac4C modifications by formaldehyde-crosslinked RIP-seq assay. The data showed that MVC RNAs were captured by the Flag-specific antibodies in Flag-NP1 transfected cells when compared with the control, indicating the NP1 bound with MVC RNA (Fig. 4A), but the mutation at residue 3311 did not alter the levels of NP1 bound RNAs after comparing the effects of transfection with 3311m to WT (Fig. 4B). Beyond the RNA binding capacities, the triple arginine/serine (SR) dipeptide motifs are in charge of NP1 mediated RNA processing [30]. To explore the potential correlation between ac4C and NP1, the SR motifs were mutated based on WT or 3311m for following analyses (Fig. 4C). Next, we determined effect of SR motifs of NP1 on viral replication by Southern blot assay, our data showed that compared to WT, the SRm did reduce MVC DNA replication (Fig. 4D, lanes 1–3). In addition, viral proteins expression was decreased by mutating SR motifs (Fig. 4E, lanes 1 and 2). These data showed that levels of both viral replication and viral proteins expression were decreased by mutating SR motifs in WT. While no synergistic effects of decreased viral replication and VP2 protein expression were observed in mutations with both SRm and 3311m (Fig. 4D, compare lane 5 to lanes 3 and 4; Fig. 4E, lane 4 to lanes 2 and 3). Whereas the mutation of SR motifs in NP1 did not change the expression of NAT10 (Supplementary Fig. S6A) and the ac4C levels of MVC RNA (Supplementary Fig. S6B), which suggested SR sequence mutations regulate viral replication not by altering NAT10 protein expression. Meanwhile, the levels of MVC transcribed pre-mRNAs were not affected by changing SR motifs, after RT-qPCR assays using three different primers targeting different coding regions (Fig. 4F and G).

To elucidate the underlying mechanisms that NP1 might directly or indirectly coordinate with ac4C to regulate MVC RNA processing, cells transfected with indicated mutants were subjected to RPA assays (Fig. 4C). Consistently, ∼6-fold decrease of alternative splicing at 3D sites (Fig. 4H, compare lane 4 to lane 3) and ∼9-fold increase of alternative polyadenylation at (pA)p (Fig. 4I, compare lane 4 to lane 3) were detected in cells transfected with SRm, compared to WT. Nevertheless, no differences of alternative splicing at 3D sites (Fig. 4H, compare lane 6 to lane 5) and alternative polyadenylation at (pA)p (Fig. 4I, compare lane 6 to lane 5) were detected in cells transfected with 3311m by mutating SR sequence. Thus, these indicated that ac4C could play a role in NP1-mediated viral RNA processing. Taken together, these results revealed that the loss of ac4C at residue 3311 did not influence the MVC RNA-binding capacity of NP1, but still participated in the NP1-mediated alternative viral RNA processing. These implied that unknown host factors were involved in the alternative viral RNA processing regulated by NP1 along with ac4C.

CPSF5 is recruited by NP1 and affects 3D/3A splicing and (pA)p polyadenylation

Tandem mass spectrometry (MS) with IP in cells with exogenous NP1 expression was conducted to identify potential host factors mediating the connection between NP1 and ac4C at residue 3311 during the MVC RNA processing (Fig. 5A). Candidates obtained via MS were ranked according to their intensity (Table 1). After screening and verification via co-IP assays, the host factor CPSF5 was found to interact with NP1 (Fig. 5A and Supplementary Fig. S7A). To further explore the roles of CPSF5 during the MVC replication, the viral genome replication and protein expression were examined after knocking down CPSF5. Our data showed that knocking down CPSF5 decreased MVC DNA replication by Southern blot assay (Fig. 5B). In addition, viral proteins expression was decreased according to the WB assays (Fig. 5C, lanes 1–3; Supplementary Fig. S7B). Thus, both the MVC genome replication and viral VP2 protein expression were inhibited by CPSF5 depletion. No additive inhibitory effects of VP2 expression were observed after depleting CPSF5 in combination with mutating residue 3311 (Fig. 5C, compare lanes 5 and 6 to lane 4). Meanwhile, the levels of transcribed VP2 and NP1 mRNAs were downregulated by CPSF5 depletion in cells transfected with WT (Fig. 5D). No additive inhibitory effects of VP2 transcripts were observed after depleting CPSF5 in combination with mutating residue 3311, but not NP1 RNA level (Fig. 5E), while NS1 mRNA was not affected (Supplementary Fig. S8A and B).

Correspondingly, we also determined the relationship between CPSF5 and MVC RNA processing in CPSF5 knockdown cells transfected with WT or mutant 3311m using RPA assays. The data showed that CPSF5 depletion inhibited the alternative splicing of the 3D/3A intron (∼10-fold) (Fig. 5F, Supplementary Fig. S8C, compare lanes 4 and 5 to lane 3), but facilitated the alternative polyadenylation at (pA)p (∼13-fold) (Fig. 5G, Supplementary Fig. S8D, compare lanes 4 and 5 to lane 3) after MVC infection or transfection with WT. However, along with mutation of residue 3311, knockdown of CPSF5 did not affect the alternative MVC RNA processing at 3D sites or (pA)p (Fig. 5F and G, compare lanes 7 and 8 to lane 6). These indicated that the CPSF5-mediated such regulatory effects were dependent on residue 3311. In addition, the RNA levels and protein expression of NAT10 were not influenced by the overexpression or knockdown of CPSF5, which suggested knockdown of CPSF5 regulated viral replication and RNA processing not by altering NAT10 protein expression (Supplementary Fig. S9). Consistent with previous studies, CPSF5 was capable to efficiently bind with MVC RNAs (Fig. 5H), and the levels of CPSF5-bound viral RNAs were decreased by substituting residue 3311 via RIP-qPCR assays (Fig. 5I). Overall, CPSF5 interacts with NP1 to regulate MVC replication and RNA processing. Different from that of NP1, the CPSF5-mediated alternative viral RNA processing appears to depend on ac4C at residue 3311, which affects the viral RNA-binding capacity of CPSF5.

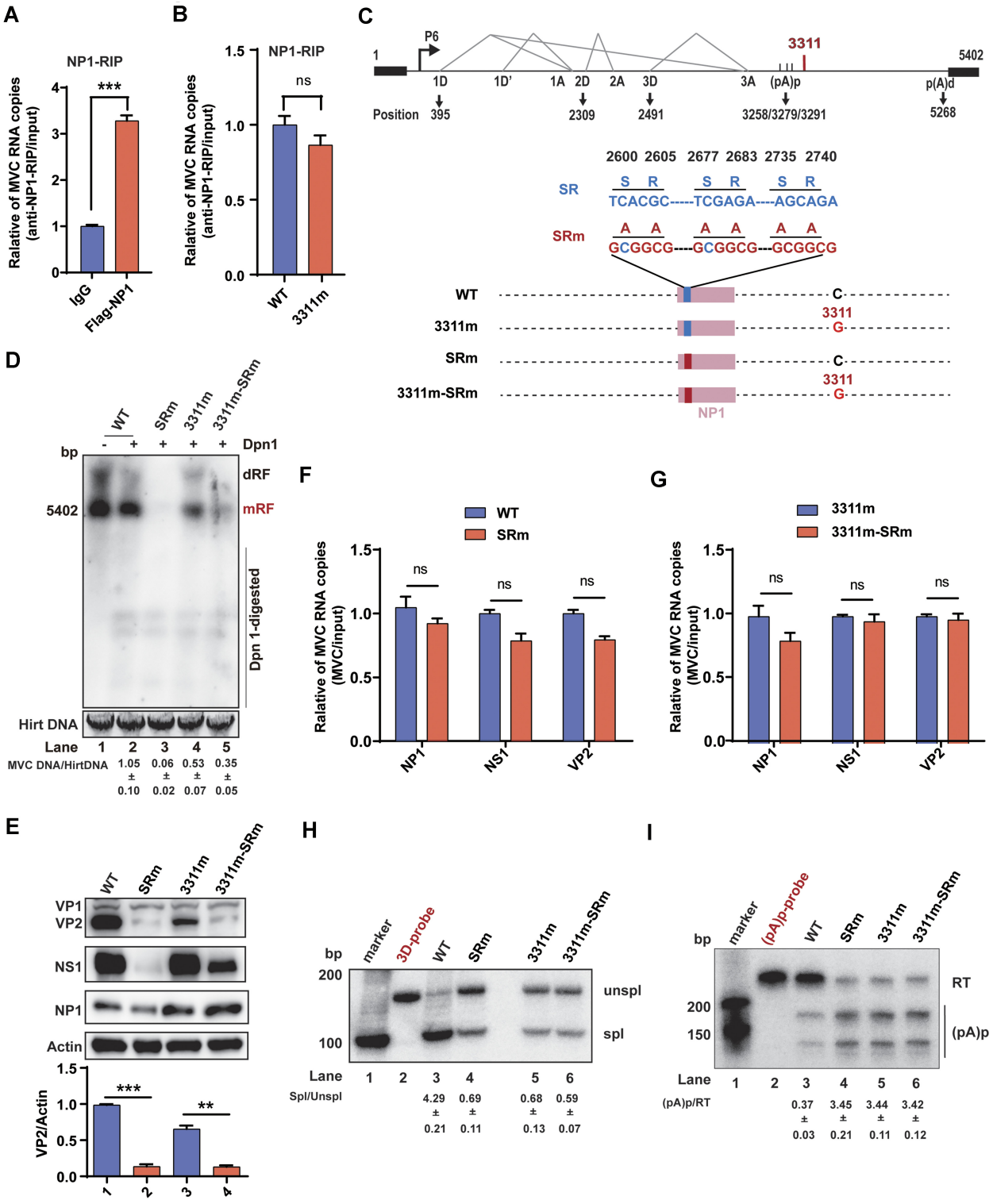

Figure 4. Ac4C at residue 3311 and NP1 are critical for the splicing at 3D site and (pA)p readthrough. (**A**, **B**) Ability of NP1 binding to the targeted MVC RNA based on formaldehyde-RIP (RNA-immunoprecipitation) and qRT-PCR. Cell lysates from formaldehyde-cross-linking were subjected to IP with IgG or anti-NP1 antibodies (**A**). WT and mutant 3311m infectious clones were used to transfect WRD cells, and cell lysates followed by formaldehyde-cross-linking, were subjected to IP with anti-NP1 antibodies (**B**). qRT-PCR was performed to quantify MVC RNA. Unpaired student's *t*-tests were performed, and the data are presented as the means ± SEMs ($n = 3$). ns: not significant, $^{***}P \leq 0.001$. (**C**) Diagram indicating the relative locations of the NP1 arginine/serine (SR) mutants and alignment of nucleotide 2600–2740 of wild-type MVC NP1 (WT, 3311m) and NP1-SRsm (WT-SRm, 3311m-SRm). (**D**) Southern blot analysis was performed to detect MVC DNA replication in cells transfected with MVC infectious clones WT, WT-SRm, 3311m, and 3311m-SRm at 48 h. (**E**) Western blot analysis of MVC protein expression in WRD cells transfected with the infectious clones, indicated as Fig. 4C; actin was used as a control. (**F**, **G**) Effect of MVC RNA level by mutating NP1 SR domain. qRT-PCR of total RNA extracted from WRD cells transfected with the same infectious clones as Fig. 4C. Data are means ± SEMs ($n = 3$). ns: not significant, unpaired Student's *t*-tests. (**H**, **I**) Correlation between NP1 and the ac4C-modified residue affected MVC RNA processing based on RPA. RPA of total RNA extracted from cells transfected with the infectious clones WT, WT-SRm, 3311m, and 3311m-SRm at 48 h were performed using a 3D-probe (**H**) and (pA)p-probe (**I**).

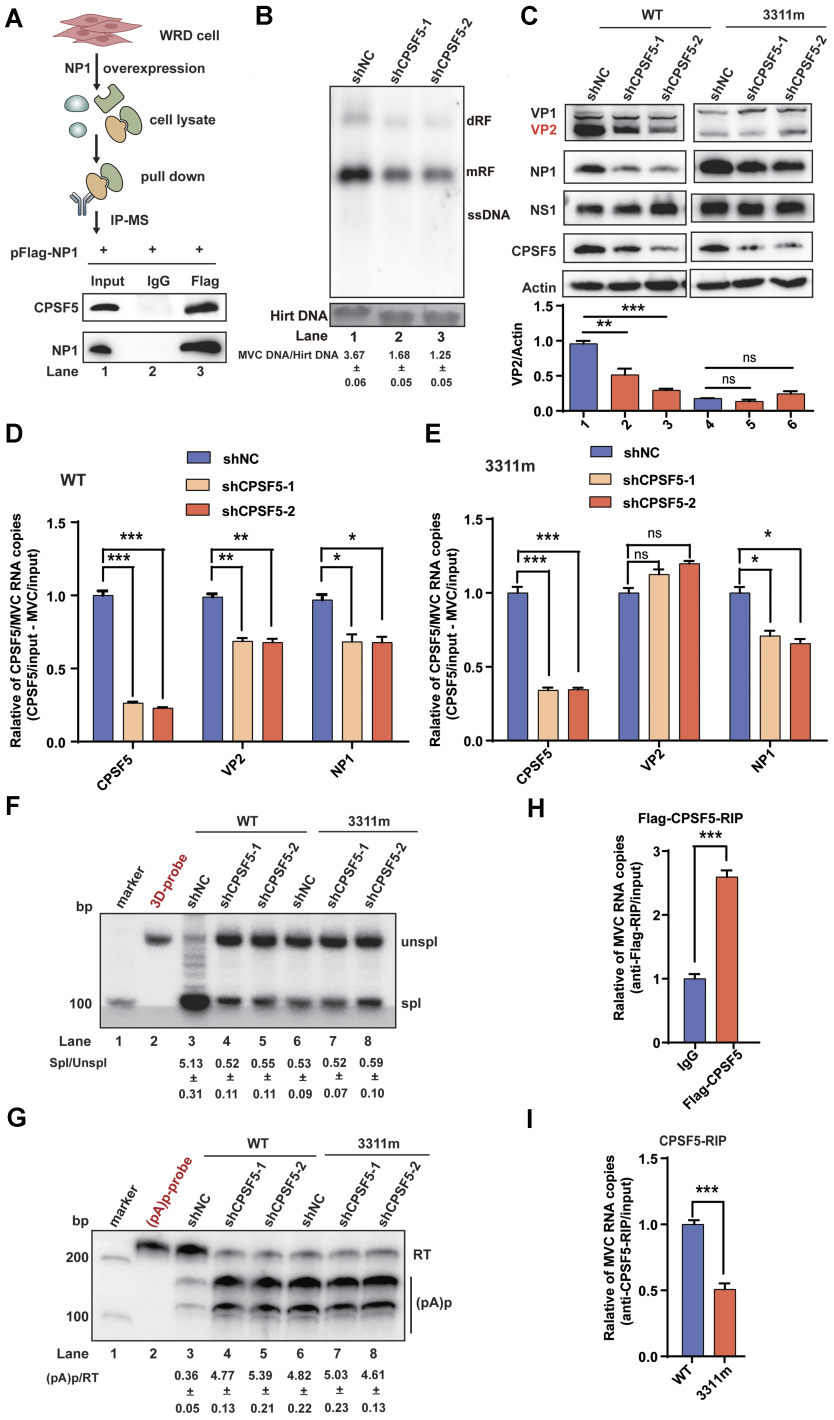

Figure 5. CPSF5 recruited by NP1 targets viral RNAs to further regulate the alternative RNA processing. (**A**) NP1 interacts with CPSF5, which was verified by performing an IP assay. Flag-tagged NP1 was transiently expressed in WRD cells and then purified by IP using anti-Flag antibodies and detected via MS (Table 1) or western blotting. IgG was used as a negative control. (**B**) Southern blot assay showing MVC DNA replication in CPSF5 knockdown cells. Hirt DNA was extracted from MVC-infected cells with CPSF5 knockdown and subjected to Southern blot analysis at 48 h post-infection. (**C**) The expression of MVC protein was identified with CPSF5 knockdown. Western blot analysis of MVC protein expression by knocking down CPSF5 in WRD cells transfected with WT or mutant 3311m MVC infectious clone at 48 h; actin was used as a control. Relative intensity of VP2 versus actin was quantified using the ImageJ program. Data are means ± SDs ($n = 3$). $^{***}P \leq 0.001$, $^{**}P \leq 0.01$, unpaired Student's *t*-test. (**D**, **E**) MVC RNA levels detected in CPSF5 knockdown cells. qRT-PCR was performed to determine the RNA levels from CPSF5 knockdown WRD cells transfected with infectious clone WT (**D**) or mutant 3311m (**E**) at 48 h by CPSF5, NP1, VP2 ORF primers, and GAPDH was used as a control. Data are means ± SEMs ($n = 3$). $^{*}P \leq 0.05$, $^{**}P \leq 0.01$, $^{***}P \leq 0.001$, ns: not significant, unpaired Student's *t*-tests. (**F**, **G**) The relationship between CPSF5 and the ac4C-modified residue in regulating RNA processing was detected by RPA. RPA of total RNA extracted from CPSF5-knockdown WRD cells transfected with WT or 3311m mutant MVC infectious clone at 48 h was performed using a 3D-probe (**F**) and (pA)p-probe (**G**). (**H**, **I**) Ability of CPSF5 binding to the targeted MVC RNA based on formaldehyde-RIP-qRT-PCR. Flag-tagged CPSF5 was expressed in WRD cells, and formaldehyde-cross-linking cell lysates were subjected to IP with IgG or anti-Flag antibodies (**H**). WT and 3311m mutant infectious clones were used to transfect WRD cells in which CPSF5 was knocked down, then the cells were subjected to IP with anti-CPSF5 antibodies. qRT-PCR was performed to quantify MVC RNA (**I**). IgG was used as a negative control. Unpaired student's *t*-tests were performed, and the data are presented as the means ± SEMs ($n = 3$). $^{***}P \leq 0.001$.

Table 1. MS data of NP1

Accession	Gene	Mw(kDa)	Length	log2 intensity F	Fold change	log2 FC	Type
Q8QQV6	NP1	21.732	186	34.34 552 699	5251.268 974	12.35 845	Bait
F1Q2G1	FAM111B	84.605	734	30.9 389 463	1465.848 733	10.51 752	Interactor
F1Q4E3	MYO5A	209.676	1801	25.94 331 018	260.5 529 739	8.025 433	Interactor
J9P492	U2AF1	27.872	240	27.16 796 552	185.9 886 181	7.539 071	Interactor
E2RQP7	RPA2	29.537	273	30.25 878 436	95.21 938 927	6.573 183	Interactor
E2R2A4	PURA	49.338	469	25.75 498 676	84.2 622 018	6.396 814	Interactor
A0A5F4CK90	PPP1CC	34.759	304	26.34 119 711	81.38 449 543	6.346 682	Interactor
F2Z4N6	SRSF3	19.33	164	26.04 117 987	79.6 317 141	6.315 271	Interactor
A0A5F4CTD1	ATP5F1C	32.938	297	25.9 375 299	65.40 938 819	6.031 426	Interactor
F1PDI8	IGF2BP2	60.109	545	25.48 597 324	56.74 770 726	5.82 649	Interactor
E2QZR7	YTHDC2	148.65	1325	25.20 385 309	54.27 898 673	5.762 322	Interactor
E2RQX1	CCDC6	53.256	478	30.39 151 242	51.76 215 501	5.693 826	Interactor
E2R436	RPA1	68.408	616	31.18 718 732	41.01 179 194	5.357 967	Interactor
E2RFC9	NCBP2	21.333	187	25.1 958 798	39.65 461 258	5.309 417	Interactor
E2R0E1	ASB7	36.011	318	24.95 947 457	38.0 998 444	5.251 713	Interactor
A0A5F4CPH4	RPA3	37.958	351	29.1 514 631	34.02 179 494	5.088 387	Interactor
J9P0K9	CLDN1	22.787	211	24.59 701 819	32.09 393 005	5.004 229	Interactor
E2R7S5	RSL1D1	54.911	490	25.75 753 223	31.62 568 991	4.983 025	Interactor
A0A5F4DI45	ANO3	104.324	896	25.26 366 779	31.12 527 393	4.960 015	Interactor
E2QUJ4	CPSF5	26.24	227	23.83 084 089	28.29 748 414	4.822 602	Interactor
Q28284	CD44	38.066	351	24.58 623 324	27.02 980 185	4.756 479	Interactor
J9NYH3	LLPH	16.862	148	24.97 954 312	25.77 485 411	4.687 892	Interactor
A0A5F4CBE4	LUC7L3	49.069	412	26.43 931 565	23.34 446 579	4.545 009	Interactor

MS was performed by IP. IP samples obtained from WRD cells transfected with a plasmid expressing pFlag-NP1 using anti-Flag antibodies or control IgG. Candidate genes were ranked according to their intensity.

ac4C at residue 3311 coordinates NP1 and CPSF5 to regulate MVC RNA processing

Viral protein NP1, ac4C at residue 3311, and CPSF5 were involved in the alternative processing of MVC RNAs, but the potential mechanisms remain unclear. To this end, RNA pull-down assays were performed with *in vitro* synthesized RNA oligomers (oMVC-WT, oMVC-3311G, and oMVC-1-5) (Supplementary Fig. S10A and Supplementary Table S1) and cell lysates to illustrate the interactions among NP1, CPSF5, and residue 3311 without ac4C modifications. The data showed that NP1 protein was pulled down by the oMVC-1, oMVC-2, and oMVC-WT RNA oligomers, suggesting NP1 preferentially targeted the *cis*-element region around 3D site and downstream of the (pA)p region (Supplementary Fig. S10B). In addition, NP1 and CPSF5 were also pulled down by the oMVC-WT, suggesting the WT RNA oligomers bound to NP1 and CPSF5 (Supplementary Fig. S10C).

We next checked how the NP1, CPSF5, and ac4C at residue 3311 coordinated to regulate alternative MVC RNA processing. The MVC infectious clones in combination with plasmids encoding NP1 or CPSF5 were transfected into cells, and the capacity of viral RNA binding to NP1 or CPSF5 was examined by RIP-qPCR. Exogenous NP1 enhanced viral RNA binding to CPSF5, which was abolished by mutating residue 3311 (Fig. 6A and B). This implied that RNA binding to CPSF5 was mediated by NP1 and that ac4C modified residue 3311 was important for such affinity of RNA to CPSF5. In contrast, the levels of NP1 bound viral RNAs were not influenced by either CPSF5 expression patterns or residue 3311 mutation (Fig. 6C and D). These indicated that NP1 facilitated CPSF5 binding to ac4C modified viral RNAs, but CPSF5 did not affect the binding of NP1. To confirm this hypothesis, triplets of 30 nt-long RNAs containing the ac4C motif CCG were *in vitro* transcribed with normal CTP or ac4CTP substrates (Fig. 6E; Supplementary Fig. S11A and B). RNA pulldown assay was performed by using oligo RNA and cell lysates or NP1 protein, and the data showed equal amounts of NP1 proteins were pulled down by oligomers with or without ac4C modifications (Fig. 6F). However, the similar assay indicated acetylated oligomer exhibited stronger affinity to CPSF5 than that of the unmodified ones in both cell lysates and cell-free reaction mix (Fig. 6G), revealing that ac4C at residue 3311 was related with the specificity and affinity of CPSF5 to viral RNAs.

The cell-free *in vitro* assays with purified proteins NP1, CPSF5, and ac4C modified oligomers were performed to reveal more details of this entire regulatory pathway. The RNA affinity of CPSF5 to the oligomer with ac4C modifications was significantly decreased compared to that in cell lysates (Fig. 6G, compare bottom panel to top panel). The levels of RNA pull-down CPSF5 were increased by the acetylated and non-acetylated oligomers in the presence of NP1 (Fig. 6H). Conversely, exogenous CPSF5 did not increase the pull-down of NP1 by indicated oligomers under the same conditions (Fig. 6I). These indicated that NP1 was capable to recruit CPSF5 for subsequent RNA binding, and the enhanced RNA binding capacity of CPSF5 mediated by NP1 *in vitro* was consistent with previous data (Fig. 6A and B). The levels of CPSF5 pulled down via acetylated oligomers were increased by the addition of NP1 proteins in a dose-dependent manner (Fig. 6J), whereas the increasing amount of CPSF5 proteins did not affect NP1 binding to acetylated oligomers (Fig. 6K). NP1 brings CPSF5 close to the MVC RNA, and NAT10 catalyzed ac4C modification at residue 3311 ensures the specific binding to CPSF5, leading to the regulation of subsequent viral RNA alternative splicing and polyadenylation.

Discussion

In this study, new roles of NAT10 and ac4C modifications in positive regulation of MVC replication and direct influence on the alternative viral RNA processing were revealed.

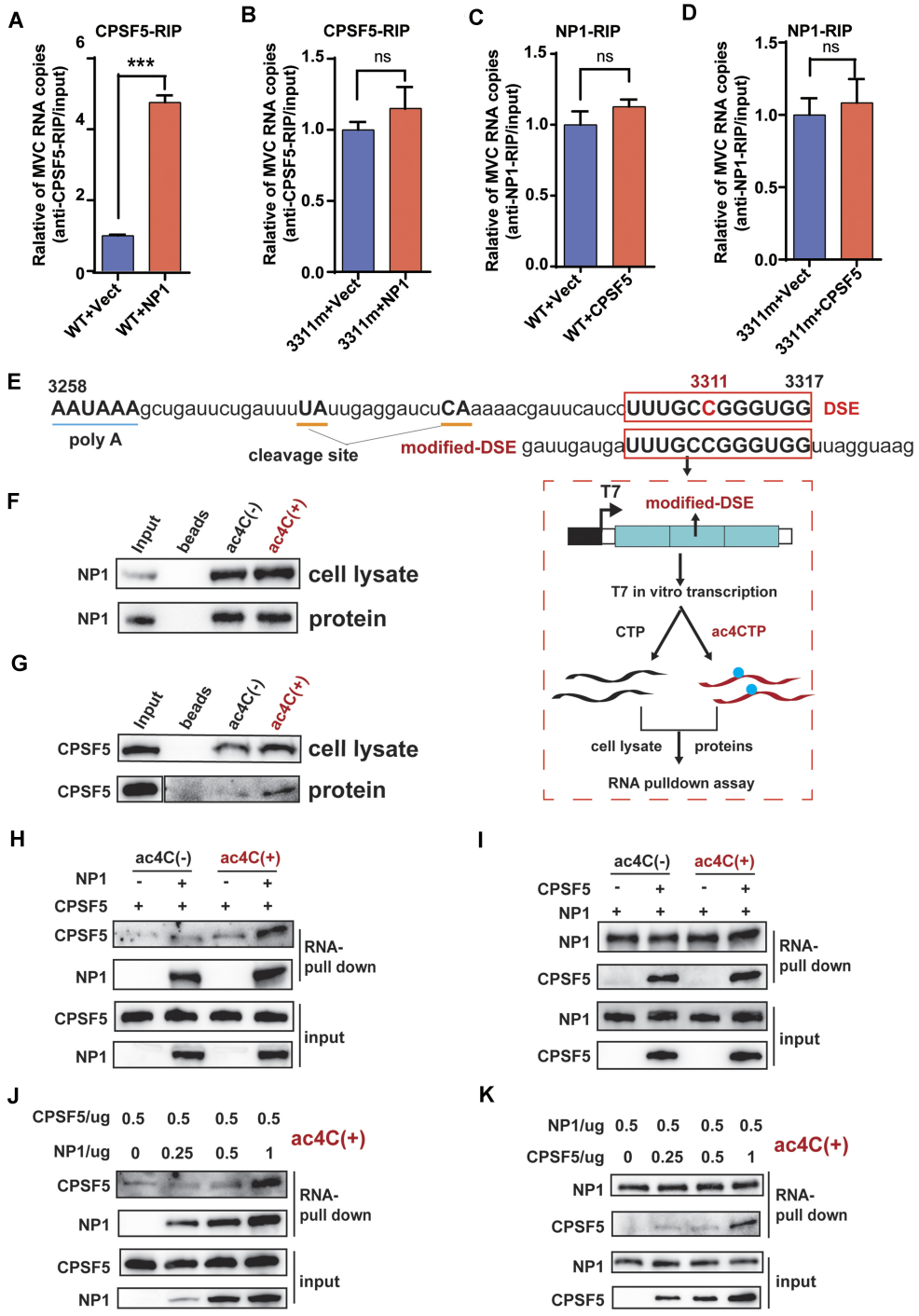

Figure 6. CPSF5 mediated MVC RNA splicing is dependent on NP1 and ac4C modification at residue 3311. (**A**, **B**) The effect on CPSF5 binding to MVC RNA by increasing NP1 expression using formaldehyde-RIP-qRT-PCR. Vector or HA-NP1 and infectious clone WT or 3311m were co-transfected in WRD cells. Cell lysates cross-linked by formaldehyde were subjected to IP with IgG, anti-CPSF5 antibodies. qRT-PCR was performed to quantify the targeted MVC RNA. IgG was used as a negative control. Unpaired Student's *t*-tests were performed, and the data are presented as means ± standard errors of the means ($n = 3$). *** $P \leq 0.001$, ns: not significant. (**C**, **D**) The effect on NP1 binding to MVC RNA by increasing CPSF5 expression using formaldehyde-RIP-qRT-PCR. Vector or Flag-CPSF5 and infectious clone WT or mutant 3311m were co-transfected in WRD cells. Cell lysates were subjected to IP with IgG, anti-NP1 antibodies. qRT-PCR was performed to quantify the targeted MVC RNA. IgG was used as a negative control. Unpaired Student's *t*-tests were performed, and the data are presented as means ± standard errors of the means ($n = 3$). ns: not significant. (**E**) Characterization of the cleavage and polyadenylation sites and downstream elements (DSEs) in (pA)p is shown at the top. The bottom panel shows a schematic representation of the RNA pulldown assay. The DNA template for T7 transcription consisted of three repeats of modified DSE. (**F**, **G**) Biotinylated RNA affinities of NP1 and CPSF5. HA-tagged NP1 or the vector was transiently expressed in WRD cells, and cell lysates were used to bind biotinylated RNA with or without the ac4C modification. In addition, purified NP1 or CPSF5 protein was mixed with RNA oligonucleotides with or without ac4C-modified RNA and analyzed via western blotting. (**H**, **I**) The binding analysis of CPSF5 or NP1 to oligo-RNA with or without the ac4C modification in the presence or absence of the NP1 (**H**) or CPSF5 (**I**) protein. (**J**, **K**) The binding analysis of NP1 and CPSF5 to ac4C-modified RNA. Equal amounts of purified CPSF5 (**J**) or NP1 (**K**) protein and increasing amounts of NP1 (**J**) or CPSF5 (**K**) protein were incubated with ac4C-modified RNA and analyzed via western blotting. Blots were detected using anti-CPSF5 or anti-NP1 antibodies.

Along with the characterization of functional ac4C-modified residue 3311 during viral replication, the mechanism was elucidated that ac4C orchestrates viral protein NP1 and host factor CPSF5 associations to regulate alternative viral RNA processing.

As the enzyme to catalyze ac4C modifications on RNAs [15], NAT10 was characterized as a new role to influence MVC RNA processing during the viral replication. The RNA stability and translation efficiency in host and different viruses [15], such as EV71 [39], HIV-1 [38], and KSHV [40, 41], are modulated by NAT10. We found NAT10 promoted MVC replication and regulated the alternative viral RNA processing. Beyond the functions of initiating protein acetylation, NAT10 mediated coordination between DNA replication and subsequent RNA processing likely existed in host cells and the replication of DNA viruses. Effects of NAT10 on host or virus RNAs are most likely mediated by its catalyzed ac4C modifications. Functional ac4C modified residues were mapped by different methods owing to their low frequency on mRNAs [16, 48, 53, 54]. To exclude potential artificial ac4C modifications on MVC RNAs, the qualitative RIP-seq and quantitative RedaC:T-seq using NaBH4 were performed, and the results were aligned. After screening several ac4C-modified residues, further mutagenesis approaches were deployed to verify the exact functional residues, which located downstream of the (pA)p motif. Subsequent *in vivo* and *in vitro* assays showed that functional ac4C on the MVC transcribed RNA specifically altered alternative splicing of the 3D/3A intron and alternative polyadenylation at (pA)p during viral RNA infection, which was differed from the previously described ac4C mediated regulation on EV71, HIV-1, and KSHV RNAs. Thus, a new role for ac4C regulating RNA processing was defined.

RNA modifications such as m6A and m5C regulate the alternative RNA processing in host cells [33, 55–57]. YTHDC1 [33], U2AF35 [3], and HNRNPA2B1 [34] target m6A modifications for binding and directly affect the subsequent RNA processing. Similarly, m5C on host mRNAs are recognized by ALYREF [56] or SRSF2 [4] for further regulation of host RNA processing. Up to date, RNA processing regulated by ac4C modification was not revealed yet. Since m5C and m6A have been revealed to involved in RNA processing, it is quite possible that these different RNA modifications might coordinate to regulate such cellular events in cells. The ac4C at residue 3311 was involved with MVC RNA processing in the current study. The indicated alternative RNA splicing of 3D/3A intron and polyadenylation at (pA)p were also mediated by the viral protein NP1. The ac4C coordinated with NP1 to regulate the viral RNA processing without changing its RNA affinity, which suggested the involvement of unknown host factors. Then, the IP tandem MS assays identified CPSF5 as a top-ranking candidate. CPSF6 had been previously reported to interact with NP1 for subsequent MVC RNA processing. As another component of the tetrameric CFIm complex, CPSF5 was revealed to potentially coordinate with NP1 to regulate subsequent viral RNA processing. Thus, NP1 may interact with CPSF5 and CPSF6 to form a complex that regulates RNA processing. The viral protein NP1 possessed specific and strong binding capacity to the MVC transcribed RNAs, while CPSF5 showed moderate and general affinity to the viral RNAs. Additional data showed that interactions between NP1 and CPSF5 largely promoted CPSF5 binding to viral RNAs. Whereas the loss of ac4C modifications at residue 3311 caused the decrease of CPSF5-bound viral RNAs. Thus, the coordination among NP1, CPSF5 and ac4C at residue 3311 ensures the efficient alternative MVC RNA processing during the viral replication.

In cells, CPSF5 binds the 5′-UGUA-3′ elements located upstream of pA signals that act as enhancers of pre-mRNA 3′-end processing [58]. In this study, the spatial and temporal working model, compromising with the viral protein NP1, host factor CPSF5 and the functional ac4C-modified residue within the DSE region, was systematically characterized. In virus life cycle, the RNA modification ac4C played an essential role for the specificity of CPSF5 targeting the DSE region for binding. Along with the enhancement of CPSF5 bound with viral RNAs by NP1, the ac4C modification at residue 3311 within the DSE region on MVC pre-mRNAs preferentially maintained the specificity of CPSF5 bound with this region. Such coordination results in the precise formation of the entire working complex to regulate alternative RNA splicing at 3D sites and polyadenylation at (pA)p. In turn, the ac4C at residue 3311 orchestrates NP1 and CPSF5 associations for efficient viral RNA processing. The binding of conserved motifs by indicated splicing factors was pivotal for host mRNA maturation. Collectively, the ac4C RNA modification ensured the specificity of the host splicing factor targeting the designated regions during the MVC replication, which further affected fine-tuned alternative splicing and polyadenylation of viral RNAs. Considering that the splicing machinery in host cells is mostly composed of a large complex, other unknown associated factors need to be identified to delineate the entire pathway.

New roles of host factor NAT10 and ac4C, along with the mechanism of RNA processing, were systematically characterized, but several unresolved points still needed to be investigated. Despite the elucidated mechanism underlying MVC replication, whether a general mechanism of ac4C-mediated RNA processing exists in host cells should be explored. Even if the host RNA metabolic machinery is deployed by viruses after infection, the mechanism by which RNA modification regulates viral RNA processing might differ from that in host cells. DNA replication, RNA transcription, and post-transcriptional modifications are strictly and precisely organized in host cells to maintain efficient and orderly RNA production and processing [59]. Collectively, this study provides new insights into the importance of RNA modifications for alternative RNA processing and helps to systematically understand the potential correlation among DNA replication, RNA transcription, and post-transcriptional modifications.

Acknowledgements

We are grateful to Lei Zhang, Ding Gao, and Juan Min of the Core Facility and Technical Support at the Wuhan Institute of Virology, CAS, for their help with next-generation sequencing, confocal microscopy, and use of isotope platforms.

Author Contributions: W.X.G., F.H. and X.Y.Z. conceptualized the study and wrote the manuscript. W.X.G., X.Y.Z., S.K.Q. and Z.C. designed and performed experiments. X.Y.Z., H.Z.L., H.J.H. and J.W. analyzed and visualized the data. W.G.X., F.H., H.J.H. and X.Y.Z. contributed with project administration, supervision and funding acquisition. All authors commented on the manuscript, participated in the data curation and approved the submitted version.

Supplementary data

Supplementary data is available at NAR online.

Conflict of interest

None declared.

Funding

This work was supported by the Strategic Priority Research Program of the Chinese Academy of Sciences [XDB0490000], Health Commission of Hubei Province scientific research project [WJ2023Z005], National Natural Science Foundation of China [32400128], Hubei Central Leading Local Science and Technology Special Project [2022BGE245], Wuhan Knowledge Innovation Special Project [2022020801020150], Wuhan Knowledge Innovation Special Project [2023020201020303], and Key R&D Program of Hubei Province [2021BCD004]. The funders had no role in the design, interpretation, or submission of this work for publication. Funding to pay the Open Access publication charges for this article was provided by Strategic Priority Research Program of the Chinese Academy of Sciences [XDB0490000] and National Natural Science Foundation of China [32400128].

Data availability

The sequence of MVC used in this work has been deposited with National Center for Biotechnology Information under accession number FJ214110.

The acRIP-seq data in Fig. 2A and RedaC:T-seq data in Fig. 2B were separately uploaded to the public database GEO (https://www.ncbi.nlm.nih.gov/geo/) with accession number GSE288473 and GSE288589.

References

1. Barbieri I, Kouzarides T. Role of RNA modifications in cancer. *Nat Rev Cancer* 2020;**20**:303–22. https://doi.org/10.1038/s41568-020-0253-2
2. Roundtree IA, Evans ME, Pan T *et al.* Dynamic RNA modifications in gene expression regulation. *Cell* 2017;**169**:1187–200. https://doi.org/10.1016/j.cell.2017.05.045
3. Mendel M, Delaney K, Pandey RR *et al.* Splice site m(6)A methylation prevents binding of U2AF35 to inhibit RNA splicing. *Cell* 2021;**184**:3125–42. https://doi.org/10.1016/j.cell.2021.03.062
4. Ma HL, Bizet M, Soares Da Costa C *et al.* SRSF2 plays an unexpected role as reader of m(5)C on mRNA, linking epitranscriptomics to cancer. *Mol Cell* 2023;**83**:4239–54. https://doi.org/10.1016/j.molcel.2023.11.003
5. Li S, Qi Y, Yu J *et al.* Nuclear aurora kinase A switches m(6)A reader YTHDC1 to enhance an oncogenic RNA splicing of tumor suppressor RBM4. *Sig Transduct Target Ther* 2022;**7**:97. https://doi.org/10.1038/s41392-022-00905-3
6. Patil DP, Chen CK, Pickering BF *et al.* m(6)A RNA methylation promotes XIST-mediated transcriptional repression. *Nature* 2016;**537**:369–73. https://doi.org/10.1038/nature19342
7. Jin T, Yang L, Chang C *et al.* HnRNPA2B1 ISGylation regulates m6A-tagged mRNA selective export via ALYREF/NXF1 complex to foster breast cancer development. *Adv Sci* 2024;**11**:e2307639. https://doi.org/10.1002/advs.202307639
8. Yang X, Yang Y, Sun BF *et al.* 5-methylcytosine promotes mRNA export—NSUN2 as the methyltransferase and ALYREF as an m(5)C reader. *Cell Res* 2017;**27**:606–25. https://doi.org/10.1038/cr.2017.55
9. Qiao Y, Sun Q, Chen X *et al.* Nuclear m6A reader YTHDC1 promotes muscle stem cell activation/proliferation by regulating mRNA splicing and nuclear export. *eLife* 2023;**12**:e82703. https://doi.org/10.7554/eLife.82703
10. Wang X, Lu Z, Gomez A *et al.* N6-methyladenosine-dependent regulation of messenger RNA stability. *Nature* 2014;**505**:117–20. https://doi.org/10.1038/nature12730
11. Chen X, Li A, Sun BF *et al.* 5-methylcytosine promotes pathogenesis of bladder cancer through stabilizing mRNAs. *Nat Cell Biol* 2019;**21**:978–90. https://doi.org/10.1038/s41556-019-0361-y
12. Liu T, Wei Q, Jin J *et al.* The m6A reader YTHDF1 promotes ovarian cancer progression via augmenting EIF3C translation. *Nucleic Acids Res* 2020;**48**:3816–31. https://doi.org/10.1093/nar/gkaa048
13. Wang Y, Wei J, Feng L *et al.* Aberrant m5C hypermethylation mediates intrinsic resistance to gefitinib through NSUN2/YBX1/QSOX1 axis in EGFR-mutant non-small-cell lung cancer. *Mol Cancer* 2023;**22**:81. https://doi.org/10.1186/s12943-023-01780-4
14. Ma CR, Liu N, Li H *et al.* Activity reconstitution of Kre33 and Tan1 reveals a molecular ruler mechanism in eukaryotic tRNA acetylation. *Nucleic Acids Res* 2024;**52**:5226–40.https://doi.org/10.1093/nar/gkae262
15. Arango D, Sturgill D, Alhusaini N *et al.* Acetylation of cytidine in mRNA promotes translation efficiency. *Cell* 2018;**175**:1872–86. https://doi.org/10.1016/j.cell.2018.10.030
16. Beiki H, Sturgill D, Arango D *et al.* Detection of ac4C in human mRNA is preserved upon data reassessment. *Mol Cell* 2024;**84**:1611–25. https://doi.org/10.1016/j.molcel.2024.03.018
17. Ito S, Horikawa S, Suzuki T *et al.* Human NAT10 is an ATP-dependent RNA acetyltransferase responsible for N4-acetylcytidine formation in 18 S ribosomal RNA (rRNA). *J Biol Chem* 2014;**289**:35724–30. https://doi.org/10.1074/jbc.C114.602698
18. Arango D, Sturgill D, Yang R *et al.* Direct epitranscriptomic regulation of mammalian translation initiation through N4-acetylcytidine. *Mol Cell* 2022;**82**:2797–814. https://doi.org/10.1016/j.molcel.2022.05.016
19. Yu C, Chen Y, Luo H *et al.* NAT10 promotes vascular remodelling via mRNA ac4C acetylation. *Eur Heart J* 2024;**46**:288–304. https://doi.org/10.1093/eurheartj/ehae707
20. Shi J, Yang C, Zhang J *et al.* NAT10 is involved in cardiac remodeling through ac4C-mediated transcriptomic regulation. *Circ Res* 2023;**133**:989–1002. https://doi.org/10.1161/CIRCRESAHA.122.322244
21. Miao D, Shi J, Lv Q *et al.* NAT10-mediated ac(4)C-modified ANKZF1 promotes tumor progression and lymphangiogenesis in clear-cell renal cell carcinoma by attenuating YWHAE-driven cytoplasmic retention of YAP1. *Cancer Commun* 2024;**44**:361–83. https://doi.org/10.1002/cac2.12523
22. Liu H, Xu L, Yue S *et al.* Targeting N4-acetylcytidine suppresses hepatocellular carcinoma progression by repressing eEF2-mediated HMGB2 mRNA translation. *Cancer Commun* 2024;**44**:1018–41. https://doi.org/10.1002/cac2.12595
23. Sharma S, Langhendries JL, Watzinger P *et al.* Yeast Kre33 and human NAT10 are conserved 18S rRNA cytosine acetyltransferases that modify tRNAs assisted by the adaptor Tan1/THUMPD1. *Nucleic Acids Res* 2015;**43**:2242–58. https://doi.org/10.1093/nar/gkv075
24. Sun Y, Chen AY, Cheng F *et al.* Molecular characterization of infectious clones of the minute virus of canines reveals unique features of bocaviruses. *J Virol* 2009;**83**:3956–67. https://doi.org/10.1128/JVI.02569-08
25. Ohshima T, Kishi M, Mochizuki M. Sequence analysis of an Asian isolate of minute virus of canines (canine parvovirus type 1). *Virus Genes* 2004;**29**:291–6. https://doi.org/10.1007/s11262-004-7430-3

26. Sukhu L, Fasina O, Burger L *et al.* Characterization of the nonstructural proteins of the bocavirus minute virus of canines. *J Virol* 2013;**87**:1098–104. https://doi.org/10.1128/JVI.02627-12
27. Schwartz D, Green B, Carmichael LE *et al.* The canine minute virus (minute virus of canines) is a distinct parvovirus that is most similar to bovine parvovirus. *Virology* 2002;**302**:219–23. https://doi.org/10.1006/viro.2002.1674
28. Tewary SK, Liang L, Lin Z *et al.* Structures of minute virus of mice replication initiator protein N-terminal domain: insights into DNA nicking and origin binding. *Virology* 2015;**476**:61–71. https://doi.org/10.1016/j.virol.2014.11.022
29. Majumder K, Boftsi M, Whittle FB *et al.* The NS1 protein of the parvovirus MVM aids in the localization of the viral genome to cellular sites of DNA damage. *PLoS Pathog* 2020;**16**:e1009002. https://doi.org/10.1371/journal.ppat.1009002
30. Fasina OO, Dong Y, Pintel DJ. NP1 protein of the *Bocaparvovirus* minute virus of canines controls access to the viral capsid genes via its role in RNA processing. *J Virol* 2016;**90**:1718–28. https://doi.org/10.1128/JVI.02618-15
31. Fasina OO, Stupps S, Figueroa-Cuilan W *et al.* Minute virus of canines NP1 protein governs the expression of a subset of essential nonstructural proteins via its role in RNA processing. *J Virol* 2017;**91**:e00260-17. https://doi.org/10.1128/JVI.00260-17
32. Dong Y, Fasina OO, Pintel DJ. Minute virus of canines NP1 protein interacts with the cellular factor CPSF6 to regulate viral alternative RNA processing. *J Virol* 2019;**93**:e01530-18. https://doi.org/10.1128/JVI.01530-18
33. Xiao W, Adhikari S, Dahal U *et al.* Nuclear m(6)A reader YTHDC1 regulates mRNA splicing. *Mol Cell* 2016;**61**:507–19. https://doi.org/10.1016/j.molcel.2016.01.012
34. Alarcon CR, Goodarzi H, Lee H *et al.* HNRNPA2B1 is a mediator of m(6)A-dependent nuclear RNA processing events. *Cell* 2015;**162**:1299–308. https://doi.org/10.1016/j.cell.2015.08.011
35. Zhu Y, Wang R, Zou J *et al.* N6-methyladenosine reader protein YTHDC1 regulates influenza A virus NS segment splicing and replication. *PLoS Pathog* 2023;**19**:e1011305. https://doi.org/10.1371/journal.ppat.1011305
36. Furuse Y. RNA modifications in genomic RNA of influenza A virus and the relationship between RNA modifications and viral infection. *Int J Mol Sci* 2021;**22**:9127. https://doi.org/10.3390/ijms22179127
37. McIntyre W, Netzband R, Bonenfant G *et al.* Positive-sense RNA viruses reveal the complexity and dynamics of the cellular and viral epitranscriptomes during infection. *Nucleic Acids Res* 2018;**46**:5776–91. https://doi.org/10.1093/nar/gky029
38. Tsai K, Jaguva Vasudevan AA, Martinez Campos C *et al.* Acetylation of cytidine residues boosts HIV-1 gene expression by increasing viral RNA stability. *Cell Host Microbe* 2020;**28**:306–12. https://doi.org/10.1016/j.chom.2020.05.011
39. Hao H, Liu W, Miao Y *et al.* N4-acetylcytidine regulates the replication and pathogenicity of enterovirus 71. *Nucleic Acids Res* 2022;**50**:9339–54. https://doi.org/10.1093/nar/gkac675
40. Yan Q, Zhou J, Wang Z *et al.* NAT10-dependent N(4)-acetylcytidine modification mediates PAN RNA stability, KSHV reactivation, and IFI16-related inflammasome activation. *Nat Commun* 2023;**14**:6327. https://doi.org/10.1038/s41467-023-42135-3
41. Yan Q, Zhou J, Gu Y *et al.* Lactylation of NAT10 promotes N(4)-acetylcytidine modification on tRNA(Ser-CGA-1-1) to boost oncogenic DNA virus KSHV reactivation. *Cell Death Differ* 2024;**31**:1362–74. https://doi.org/10.1038/s41418-024-01327-0
42. Zhang X, Guo J, Xu H *et al.* NS1-mediated enhancement of MVC transcription and replication promoted by KAT5/H4K12ac. *J Virol* 2024;**98**:1362–74. https://doi.org/10.1128/jvi.01695-23
43. Chimnaronk S, Suzuki T, Manita T *et al.* RNA helicase module in an acetyltransferase that modifies a specific tRNA anticodon. *EMBO J* 2009;**28**:1362–73. https://doi.org/10.1038/emboj.2009.69
44. Guan W, Cheng F, Yoto Y *et al.* Block to the production of full-length B19 virus transcripts by internal polyadenylation is overcome by replication of the viral genome. *J Virol* 2008;**82**:9951–63. https://doi.org/10.1128/JVI.01162-08
45. Liu X, Hao S, Chen Z *et al.* The 5′untranslated region of human bocavirus capsid transcripts regulates viral mRNA biogenesis and alternative translation. *J Virol* 2018;**92**:e00443-18. https://doi.org/10.1128/JVI.00443-18
46. Ganaie SS, Qiu J. Recent advances in replication and infection of human parvovirus B19. *Front Cell Infect Microbiol* 2018;**8**:166. https://doi.org/10.3389/fcimb.2018.00166
47. Hao H, Hao S, Chen H *et al.* N6-methyladenosine modification and METTL3 modulate enterovirus 71 replication. *Nucleic Acids Res* 2019;**47**:362–74. https://doi.org/10.1093/nar/gky1007
48. Thomas JM, Briney CA, Nance KD *et al.* A chemical signature for cytidine acetylation in RNA. *J Am Chem Soc* 2018;**140**:12667–70. https://doi.org/10.1021/jacs.8b06636
49. Liu R, Wubulikasimu Z, Cai R *et al.* NAT10-mediated N4-acetylcytidine mRNA modification regulates self-renewal in human embryonic stem cells. *Nucleic Acids Res* 2023;**51**:8514–31. https://doi.org/10.1093/nar/gkad628
50. Wang S, Li H, Lian Z *et al.* The role of RNA modification in HIV-1 infection. *Int J Mol Sci* 2022;**23**:7571.
51. Dang Y, Li J, Li Y *et al.* N-acetyltransferase 10 regulates alphavirus replication via N4-acetylcytidine (ac4C) modification of the lymphocyte antigen six family member E (LY6E) mRNA. *J Virol* 2024;**98**:e0135023. https://doi.org/10.1128/jvi.01350-23
52. Larrieu D, Britton S, Demir M *et al.* Chemical inhibition of NAT10 corrects defects of laminopathic cells. *Science* 2014;**344**:527–32. https://doi.org/10.1126/science.1252651
53. Sas-Chen A, Thomas JM, Matzov D *et al.* Dynamic RNA acetylation revealed by quantitative cross-evolutionary mapping. *Nature* 2020;**583**:638–43. https://doi.org/10.1038/s41586-020-2418-2
54. Thalalla Gamage S, Sas-Chen A, Schwartz S *et al.* Quantitative nucleotide resolution profiling of RNA cytidine acetylation by ac4C-seq. *Nat Protoc* 2021;**16**:2286–307. https://doi.org/10.1038/s41596-021-00501-9
55. Yue Y, Liu J, Cui X *et al.* VIRMA mediates preferential m(6)A mRNA methylation in 3′UTR and near stop codon and associates with alternative polyadenylation. *Cell Discov* 2018;**4**:10. https://doi.org/10.1038/s41421-018-0019-0
56. Wang N, Chen RX, Deng MH *et al.* m(5)C-dependent cross-regulation between nuclear reader ALYREF and writer NSUN2 promotes urothelial bladder cancer malignancy through facilitating RABL6/TK1 mRNAs splicing and stabilization. *Cell Death Dis* 2023;**14**:139. https://doi.org/10.1038/s41419-023-05661-y
57. Pendleton KE, Chen B, Liu K *et al.* The U6 snRNA m(6)A methyltransferase METTL16 regulates SAM synthetase intron retention. *Cell* 2017;**169**:824–35. https://doi.org/10.1016/j.cell.2017.05.003
58. Yang Q, Gilmartin GM, Doublié S. Structural basis of UGUA recognition by the Nudix protein CFI(m)25 and implications for a regulatory role in mRNA 3′ processing. *Proc Natl Acad Sci USA* 2010;**107**:10062–7. https://doi.org/10.1073/pnas.1000848107
59. Manning KS, Cooper TA. The roles of RNA processing in translating genotype to phenotype. *Nat Rev Mol Cell Biol* 2017;**18**:102–14. https://doi.org/10.1038/nrm.2016.139

Received: November 13, 2024. **Revised:** February 7, 2025. **Editorial Decision:** March 6, 2025. **Accepted:** March 12, 2025